# Universal depinning force fluctuations of an elastic line: Application to finite temperature behavior

Damien Vandembroucq, Rune Skoe, Stéphane Roux

# Universal depinning force fluctuations of an elastic line:
## Application to finite temperature behavior

Damien Vandembroucq, Rune Skoe and Stéphane Roux

*Unité Mixte CNRS/Saint-Gobain "Surface du Verre et Interfaces"*
*39 Quai Lucien Lefranc, 93303 Aubervilliers cedex, FRANCE*

The depinning of an elastic line in a random medium is studied *via* an extremal model. The latter gives access to the instantaneous depinning force for each successive conformation of the line. Based on conditional statistics the universal and non-universal parts of the depinning force distribution can be obtained. In particular the singular behavior close to a (macroscopic) critical threshold is obtained as a function of the roughness exponent of the front. We show moreover that the advance of the front is controlled by a very tenuous set of subcritical sites. Extension of the extremal model to a finite temperature is proposed, the scaling properties of which can be discussed based on the statistics of depinning force at zero temperature.

## I. INTRODUCTION

The depinning of elastic interfaces allows to describe the phenomenology of a variety of physical phenomena such that the motion of a wetting contact line on a disordered substrate[1], the propagation of a fracture front [2] in a heterogeneous material or the advance of a magnetic wall in a thin layer[3]. The depinning transition can be seen as a non equilibrium critical phenomenon (see Ref. [4, 5, 6] for recent reviews). The system is driven by an equivalent external force (the magnetic field for the domain wall, the stress intensity factor for the fracture front...) which plays the role of a control parameter. The richness of the phenomenology arises from the competition between the disordering effect of the quenched pinning potential and the ordering (smoothing) effect of the elastic forces acting on the front. The nature (short range/long range) of the latter will directly affect the universality class of the depinning. Moreover depending on the strength of the disorder, the motion front will either be collective (weak pinning) or consists of successive avalanches (strong pinning). In the following we focus on the latter situation.

To study the pinning/depinning transition, a specific algorithm has been introduced under the generic name of "extremal model" [7, 8, 9, 10]. It consists in adapting the driving force so that only one site (the weakest one) can depin at a time. In so doing, the system is compelled to stay at the edge of the critical state (the front is driven at an infinitely low velocity). Thus the evolution consists in a series of equilibrium positions, because the driving force is adjusted to meet this condition. It thus can be seen as an ideal quasi-static driving[11]. However, the price to pay in such a description, is that the dynamical aspects of the propagation are not accounted for (see Ref. [12] for details on this subject). In a more complete picture either inertia or viscosity would have to be introduced. As dynamics is scarifies, time metric is not included in the "extremal model" description. What is preserved is simply the ordering of successive configurations.

Close but below threshold, at finite temperature, an Arrhenius activation mechanism can allow for a steady "subcritical" propagation. Note that this situation differs from the creep regime at very low forcing which has been extensively studied in recent years [13, 14, 15, 16]. In the latter, the driving force is very close to zero and thermal activation may allow back and forth motion along the direction of propagation. Close to threshold however, we may neglect the probability of a backward motion. Moreover in the context of fracture or wetting, chemical reactions may produce an irreversible motion of the front. In the following we will not consider the possibility of front receding. The activated mechanism thus turns out to be relatively easy to implement as an extension of the extremal model, where the latter is recovered in the limit of zero temperature. The motion consists in a succession of fast moves interrupted by long trapping events which require a thermal activation step to overcome an energy barrier. If the temperature is very low compared to the trap depths, the first site to depin will be the weakest one. In this limit of a vanishing temperature the system will thus naturally follow an *extremal* dynamics. The degeneracy of the time metric can however be clarified by studying the zero temperature limit. This description is valid for a subcritical forcing, close to threshold. This forcing introduces a finite correlation length. However, the thermal activation itself introduces another finite correlation length. The competition between these two length scales will finally control the scaling property of the propagation.

The aim of this paper is thus a careful study of the effect of temperature on both the dynamics and the critical properties of the depinning fronts. A key parameter in the finite temperature depinning is the ratio between the thermal energy and the trap depths all over the front. The latter directly depend on the fluctuations of the depinning forces at zero temperatures. The external force needed to depin the front from a blocked configuration is actually a highly fluctuating quantity. The knowledge of the distribution of these depinning forces thus appears to be an essential ingredient in the study of depinning at finite temperature.

The first part of this paper is thus devoted to the study of the depinning forces at zero temperature. We

show in particular that the distribution of depinning forces presents some universal features close to the critical threshold. A criterion characterizing the transition between low and high temperature behavior requires additional information about the distribution of trap depths along the front. Again we show that this distribution presents some universal features. In the second part we introduce a Monte-Carlo like algorithm allowing to drive the front under constant forcing at finite temperature. We briefly present results concerning the two limiting cases (at low and high temperatures) and finally focus on the transition between the two regimes. The role of the two competing correlation lengths governed respectively by the driving force and the temperature will be discussed in this last section.

## II. DEPINNING FORCE DISTRIBUTIONS

### A. Description of the model

At each time step, the front is represented as a single valued function $h(x)$, with the additional assumption that its slope is small. The mean orientation of the front is along the $x$ axis, while it propagates along a perpendicular direction $y$. For numerical simulations, the front is discretized on a regular grid of size $L$ with periodic boundary conditions: $h_i = h(x_i)$.

Time is also discretized and incremented by one unit at each elementary move of the front. This time is thus a simple way to order the successive events, but it does not correspond to a physical time. Additional information has to be introduced to describe the off-equilibrium motion, and thus decide whether viscosity or inertia, or activation processes control the dynamics. The strength and weakness of the extremal approach is that only successive static positions are described, while the transition between these conformations becomes part of the postulated rules of the model but do not stand for a real dynamic. Thus in this first part, $t$ should not be misinterpreted as a real time. However, in the finite temperature section, we will come revisit this question and see how the extremal dynamics can be recovered with a more realistic dynamics.

As introduced above, the motion of the front driven at an external force $F$ depends only on the competition between a local trapping force $\gamma(x, h(x))$ and an elastic interaction $F^{el}(x)$. We now specify them in more details.

The distortion of the front due to the random environment induces elastic restoring forces. In the case of wetting the latter are the capillary forces. Using a small slope approximation, the elastic force contribution is linear w.r.t. $h(x)$, $F^{el}(x) = \int G(x-x')h(x')\mathrm{d}x'$. Depending on the physical situation considered, these interactions can be short or long ranged. In the case of wetting the kernel $G$ presents an algebraic decay $G(r) \propto r^{-2}$ up to the capillary length. In a Hele-Shaw experiment however, the cut-off scale of the capillary forces is given by

the width of the cell and the Green function can be approximated by $G \simeq \delta''$, the second derivative of the Dirac distribution $\delta$. These short ranged interactions are then well described by a Laplacian term. In the following we focus on the latter situation with $F^{el} \propto -\partial^2 h/\partial x^2$, or in the discretized version, $F_i^{el} = -h_{i-1} + 2h_i - h_{i+1}$.

The randomness of the environment can be introduced in two respects: first in the spatial distribution of the traps, second in the distribution of the trap depths. No correlation is considered here and these two quantities entirely characterized by their statistical distribution. Note that the same critical behavior is obtained as soon as either the trap positions or the trap depths are random. Either one of these two quantities can be a constant without changing the universality class of the model, i.e. all critical properties remain unaffected. We have performed a number of different numerical simulations changing the shape of the two distributions, and the only changes which are observed concerns small scales in space and time. In the following we will consider that the trap depth $\gamma(x, h(x, t))$ and the front advance at the active site are uniformly sampled between 0 and 1.

In order to study the depinning force fluctuations, we drive the system with an extremal dynamics. This consists in adapting the external force so that only one site can depin at each iteration step. For a given external force $F$, the criterion for depinning at a particular position $i$ on the front is

$$F > F_i(t) = \gamma_i(h_i(t)) + F_i^{el}(\{h_j(t)\}) \qquad (1)$$

One can thus naturally define the extremal site $(i^*, h_{i*})$ such that $F_c(t) = \min_i F_i(t) = \gamma_{i*} + F_{i*}^{el}$ is the minimal external force to apply so that at least one site of the front can depin. The depinning criterion for a particular conformation of the front is thus

$$F > F_c(t) = \min_i \left[ \gamma_i(h_i(t)) + F_i^{el}(\{h_j(t)\}) \right] \qquad (2)$$

The front depinning force $F_c(t)$ is in our simple version totally controlled by the front geometry. The extremal dynamics simply consists in tuning at each iteration step $t$ the external force at exactly the depinning force of the current front conformation : $F(t) = F_c(t)$. From the dynamical point of view it corresponds to drive the front at vanishing velocity with a very stiff spring. The system thus remains constantly at the edge of the critical state. The front explores a large number of different configurations to which correspond fluctuations of the depinning force $F_c(t)$. By definition the critical threshold $F^*$ is the minimum constant force to apply so that the front can advance indefinitely, it thus corresponds to the maximum of the front depinning force $F_c$ over all conformations:

$$F^* = \max_t F_c(t) = \max_t \left[ \min_i \left[ \gamma_i(h_i(t)) + F_i^{el}(\{h_j(t)\}) \right] \right] \qquad (3)$$

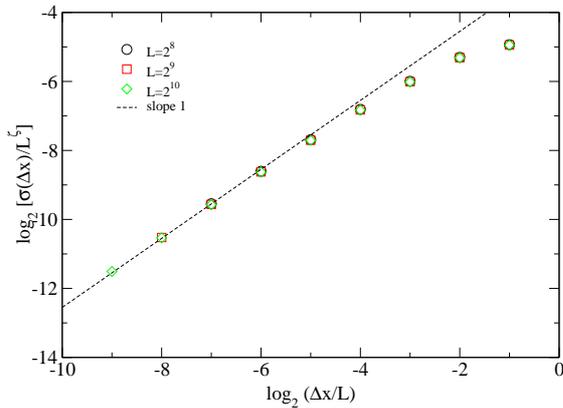From the numerical point of view, the extremal dynamics finally amounts to iterate the following sequence:*i)*

FIG. 1: Standard deviation $\sigma(\Delta x)$ of the height difference between points separated by a distance $\Delta x$ for different system sizes $L = 2^8, 2^9, 2^{10}$. The rescaling $x \to x/L$, $\sigma \to \sigma/L^{\zeta-1}$ with $\zeta = 1.25$ allows to capture the finite size effects.

identify the extremal site $i^*$; *ii)* advance the front at position $i^*$ by a random increment; *iii)* update the trap depth, $\gamma_{i*}$ on the site $i^*$ corresponding corresponding to the new front position $h(i^*)$; *iv)* update the elastic couplings $F_i^{el}$ on the front to account for this local advance. The most time consuming step is the identification of the extremal site. Numerically efficient implementation can be used to reduce the computation cost of each iteration to $\log_2(L)$ operations because of the short range nature of the interaction (note that in case of long range interactions, introducing an ultrametric distance along the front [17] allows to reach the same numerical efficiency without changing the universality class of the model).

## B. Scaling properties

Let us summarize the expected scaling behaviors for an elastic line driven at a constant force $F$ close to (but below) threshold $F^*$.

- Below threshold $F^*$ the length of the typical advance $\xi_\perp$ scales as $\xi_\perp \propto (F^* - F)^{-\nu_\perp}$

- The correlation length along the front scales as $\xi_\parallel \propto |F^* - F|^{-\nu_\parallel}$.

- The relaxation time $\tau$ of a line segment of length $\xi$ scales as $\tau \propto \xi_\parallel^z$; $z$ is called the dynamic exponent.

- At threshold, in the steady state, the front conformation is self-affine, characterized by a roughness exponent $\zeta$. This can be shown by studying the average power spectrum of the front which scales as $k^{-1-2\zeta}$. Similarly the wavelet transform also reveals the same exponent[18]. In real space, the typical width $w$ (r.m.s. height) of the front over an interval $\Delta x$ scales as $w(\Delta x) \propto (\Delta x)^\zeta$, when $\zeta$ is smaller or equal to 1. This is observed

for some long-range elastic kernel. In our case, where the elastic kernel is the local curvature, we will see below that the $\zeta$ exponent is larger than unity. In this "super-roughening" case, the scaling is anomalous[19] and the previous relation has to be corrected to $w(\Delta x) \propto L^{\zeta-1}\Delta x$. On Fig. 1 we show numerical evidence for the validity of this "super-rough" scaling with the value $\zeta = 1.25$ for the roughness exponent.

- Close to the critical threshold the motion consists of successive localized avalanches of lateral size $\Delta x$. The size distribution of these jumps follows a power law up to the correlation length $\xi_\parallel$. Below $\xi_\parallel$, the probability of observing jumps of size $\Delta x > \ell$ scales as $P(\Delta x > \ell) \propto \ell^{-1-A}$. In the framework of an extremal dynamics driving, the driving force is not constant but is adjusted at the current depinning force $F_c(t)$. An avalanche triggered at a force $F$ thus corresponds to a sequence of depinning events such that the current depinning force remains below the driving force $F_c(t) < F$. The distributions of avalanches can thus be directly derived from the fluctuations of this depinning force $F_c(t)$. A directly related quantity is the probability $P(\Delta x|\tau')$ that after a sequence of $\tau'$ events the depinning site has moved a distance $\Delta x$. We have

$$P(\Delta x|\tau') \propto \Delta x^{-a}\phi\left(\frac{\Delta x}{\tau'^{1/z'}}\right) \quad (4)$$

where $\phi(u) \propto u^a$ for $u \ll 1$ and $\phi(u) \approx$ cste for $u \gg 1$. In the framework of extremal dynamics, $z'$ corresponds to a dynamic exponent (see Ref. [12, 20] for details on the relations between $z'$ and the genuine dynamic exponent $z$ introduced above. In the following we restrict the study to extremal dynamics and we use the notation $z$ for the sake of simplicity.

Simple scaling relationships immediately derive from these properties and allow to reduce the number of independent exponents.

- Below threshold the front advance is confined to a region of length $\xi_\parallel$, and in the case of a roughness exponent $\zeta > 1$ the mean advance over this region is of order $\xi_\perp \propto \xi_\parallel L^{\zeta-1} \propto (F - F^*)^{-\nu_\parallel} L^{\zeta-1}$. This leads to

$$\nu_\perp = \nu_\parallel = \nu$$

with an unusual size-dependent prefactor. Note that this property is only true for a roughness exponent $\zeta > 1$, otherwise $\nu_\perp = \nu_\parallel \zeta$.

- Over a region of extent $\xi_\parallel$, the typical macroscopic curvature is of order $\xi_\parallel^{\zeta-2}$, and the latter scaling should balance the fluctuation of depinning force
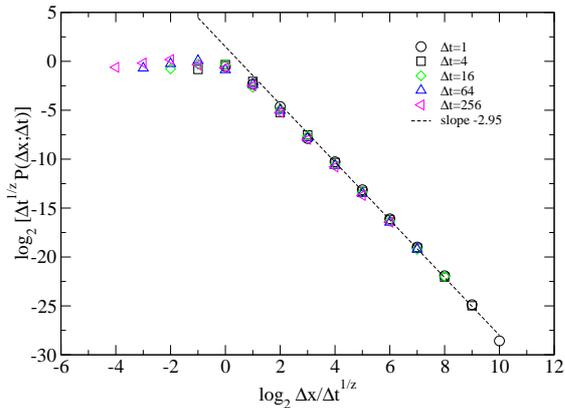
FIG. 2: Distribution of distances between active sites corresponding to depinning events separated by a time delay between $\Delta t = 1$ and $\Delta t 2^5$. After rescaling all distributions fall on a master curve. This rescaling has been obtained with the value $z = 2$ for the dynamic exponent. The dashed line corresponds to a power law of exponent $a = -2.95$
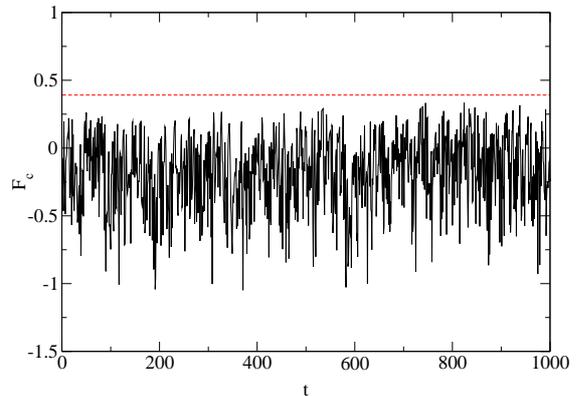


FIG. 3: Sequence of depinning forces $F_c(t)$. The dashed line corresponds to the value of the critical threshold $F^* = \max_t F_c(t)$

observed in order to depin such a segment: $\Delta F \propto \xi_{\parallel}^{-1/\nu}$. Therefore[5]

$$\zeta + \frac{1}{\nu} = 2 \qquad (5)$$

• Let us recall that time only counts individual motions, and is not physical. Therefore the dynamic exponent is an improper denomination. Nevertheless, in this section, we keep this denomination since it refers to its common usage in statistical models.

The mean advance of a segment of length $\xi$ scales as $L^{\zeta-1}\xi$ and the size of an avalanche of lateral extension $\xi$ writes $\tau \propto \xi^2 L^{\zeta-1}$ which leads immediately to

$$z = 2 \qquad (6)$$

whenever $\zeta > 1$. Note however that even if the dynamic exponent $z = 2$ appears to be super-universal as soon as $\zeta > 1$, the relation between $\tau$ and $\xi$ becomes system size dependent. Otherwise, for $\zeta < 1$, the same argument leads to $z = 1 + \zeta$[10, 20].

All exponents but $a$ which characterizes the avalanche behavior can then be directly derived from the roughness exponent $\zeta$. An simple scaling relationship can however be established in the context of the avalanches[21]. Let us start from the probability $P(\Delta x|\tau)$ that after a sequence of $\tau$ events the depinning site has moved from a distance $\Delta x$. The distance $\Delta x$ is nothing but the sum of all successive jumps $\Delta y_i$ occurring at steps $i \in [1, \tau]$. The distribution of these jumps being $P(\Delta y) \propto (\Delta y)^{-a}$. Assuming no time correlation we can apply a generalized central limit theorem for the sum variable $\Delta x$. The value

of the exponent $a$ being slightly below 3, the limit distribution is not Gaussian but a Lévy distribution $\mathcal{L}_{a-1}$ that exhibits at infinity the same power law behavior as the original power law distribution:$\mathcal{L}_{a-1}(\Delta x) \propto (\Delta x)^{-a}$:

$$P(\Delta x, \tau) \approx \frac{1}{\tau^{\frac{1}{a-1}}} \mathcal{L}_{a-1}\left(\frac{\Delta x}{\tau^{\frac{1}{a-1}}}\right) \qquad (7)$$

which leads to the scaling relationship $a = 1 + z$. In the present case of Laplacian elasticity, $z = 2$ and the prediction $a = 3$ slightly overestimates the value obtained by numerical simulations $a \approx 2.95$ (see Fig. 2. This good agreement can be interpreted as the quasi absence of temporal correlations. Note however that in the case of long range elasticity where the role of temporal correlations is expected to be higher, this scaling relationship becomes $a = 2 + \zeta$ which is far above the measured values $a \approx \alpha$ where $\alpha$ is the exponent of the elastic redistribution function. In the latter case, temporal correlations become more significant.

## C. Scaling and universality of depinning forces fluctuations

On Fig. 3 we display a sequence of depinning forces $F_c(t)$ observed over 1000 steps of an extremal dynamics simulation and the corresponding distribution $P(F_c)$ in Fig. 4. The upper force value of this distribution corresponds to the critical threshold $F^*$. In the following we will argue that close to the critical threshold the distribution of depinning forces exhibits a universal behavior:

$$P(F_c) \propto (F^* - F_c)^{\mu} \qquad (8)$$

Let us come back now to the series of depinning events. The depinning force $F_c$ fluctuates and can be described by a statistical distribution. The maximum value of the latter gives the value of the critical threshold. In the framework of a simulation this threshold $F^*$ is obtained
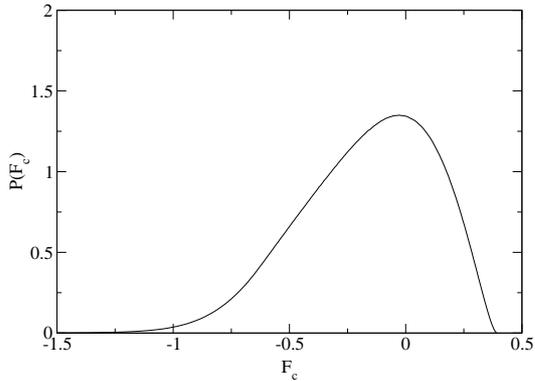
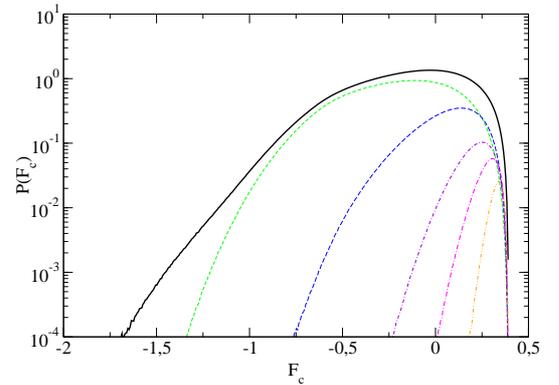FIG. 4: Distribution of depinning forces, $p(F_c)$.



FIG. 5: Distribution of depinning forces conditioned by their distance to threshold, $p(F_c, d)$, and the resulting global distribution $P(F_c)$ (bold). The larger the distance $d$ between consecutive active sites, the narrower the distributions and the closer to the critical force.
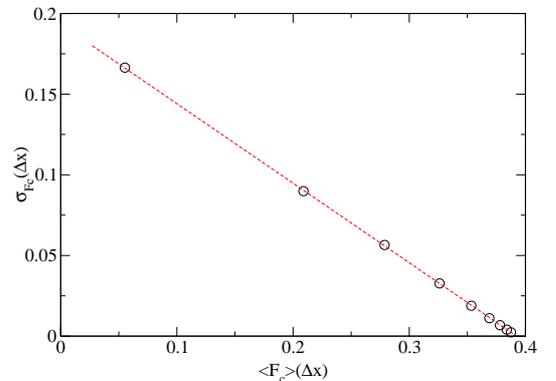


FIG. 6: The linear relationship between the mean depinning force and its fluctuation allows to extrapolate the value of the depinning force for an infinite distance between consecutive active sites *i.e.* the depinning threshold $F^*$ for an infinite system. A numerical fit gives $F^* = 0.392 \pm 0.002$.

as the maximum depinning force over the ensemble of depinning events. Restricting ourselves to a finite system of lateral extension $L$, our determination will be biased by finite size effects. This invites us to introduce a simple prescription to get a very accurate determination of $F^*$. Conditioning the distribution of depinning force by the distance $d$ between consecutive active sites, we can built distributions $P(F_c; d)$. We expect these distributions to converge to a Dirac distribution centered at $F^*$ as $d$ diverges since we probe only critically pinned configurations. This effect is directly observed on Fig. 5 where we superimpose the original distribution of depinning forces $P(F_c)$ and the contributions corresponding to increasing jump sizes $d$. We observe that, except for small jumps the successive distributions keep a similar shape up to scaling factors. In the following we check that these conditional distributions can indeed be rescaled onto a unique master curve using the scaling:

$$P(F_c; d) = \frac{1}{d^{-b}} \psi \left( \frac{F^* - F_c}{d^{-b}} \right) \qquad (9)$$

As a direct consequence of such a scaling we should in particular observe that the first and second cumulant of these distributions *i.e* the difference $F^* - \langle F_c \rangle$ and the standard deviation both scale as $d^{-b}$:

$$\delta F_c(d) = F^* - \langle F_c \rangle(d) \propto d^{-b} , \qquad (10)$$
$$\sigma_{F_c}(d) = \sqrt{\langle F_c^2 \rangle(d) - \langle F_c \rangle^2(d)} \propto d^{-b} \qquad (11)$$

This scaling directly leads to a linear dependence between $\langle F_c(d) \rangle$ and $\sigma_{F_c}(d)$. On Fig. 6, we check indeed that for large values of the jump size $d$, this linear behavior is obeyed. By extrapolation of this linear relationship for an infinite system for which the width $\sigma_{F_c}(d)$ cancels, we obtain a precise determination of the critical threshold $F^*$. We obtain in the present case

$$F^* = 0.392 \pm 0.001 \qquad (12)$$

Using the latter value we plot on Fig. 7 the evolution of $\delta F_c(d)$ and $\sigma_{F_c}(d)$ versus $d$ in logarithmic scale. The

observed linear behavior corresponds to power laws of exponent $b = 0.75$. The value of the latter exponent can be understood since the depinning force $F_c$ directly derives from the local curvature. The latter can be estimated using the elastic kernel and the roughness of the front. In the present case we have $\delta F^{el}(d) \propto d^{\zeta - 2}$ where $\zeta \approx 1.25$ is the roughness exponent of the depinning front. This estimation $b = 2 - \zeta \approx 0.75$ is consistent with our numerical data. Moreover we can identify $1/b$ to the exponent $\nu$ characterizing the divergence of the correlation length close to threshold and we recover the scaling law of Eq. (5):

$$\zeta + \frac{1}{\nu} = 2 \qquad (13)$$

Using this scaling we check on Fig. 8 that the successive conditional distribution collapse onto a single universal master curve. The knowledge of the distribution

of distances between successive depinning sites allows us now to derive the behavior of the force distribution close to threshold.

$$
\begin{aligned}
P(F^* - F_c) &= \int P(F_c; \ell) p(\ell) \mathrm{d}\ell \\
&= \int \ell^{\frac{1}{\nu}} \psi \left[ (F^* - F_c)\ell^{\frac{1}{\nu}} \right] \ell^{-a} \mathrm{d}\ell \\
&= (F^* - F_c)^{-1 + a\nu - \nu} \int u^{1 - a\nu + \nu - 1} \psi(u) \mathrm{d}u \\
&\propto (F^* - F_c)^{(a-1)\nu - 1}
\end{aligned}
\tag{14}
$$

We thus obtain a universal behavior of the distribution of depinning forces $F_c$ close to threshold as presented in Eq. 8, with

$$
\mu = (a-1)\nu - 1 \approx 1.6 \tag{15}
$$

Note in addition that when the distance $d$ is small compared to the correlation length $\xi$, $x \equiv d/\xi \ll 1$, the dependence of the $P$ distribution w.r.t. $(F^* - F_c)$ should be independent of $d$, so that $P(F_c; d)$ and $P(F_c)$ share the same behavior (see Fig.5). Hence, we expect $\psi(x) \sim x^\mu$ for $x \ll 1$, in good agreement with the behavior shown on Figure 8.

At this point it is important to clarify that the distribution $P$ by itself is not universal and depends on the local definition of the front advance and the trap depth. The details of the random distributions are absorbed in the small time and scale behavior. In contrast collective effects contribute to large jumps in the active sites and $\Psi$ is universal as well as the singular behavior of $P$ close to threshold.
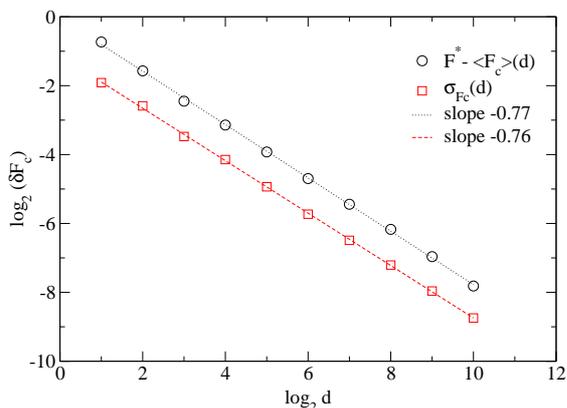


FIG. 7: The mean distance from the depinning force to the depinning threshold and the depinning force fluctuations calculated for given distances between consecutive active sites obey a scaling law with the latter distance. The straight lines plotted as a guide to the eye correspond to power laws of exponent 0.76 and 0.77 consistent with the expected value $2 - \zeta \approx 0.75$.
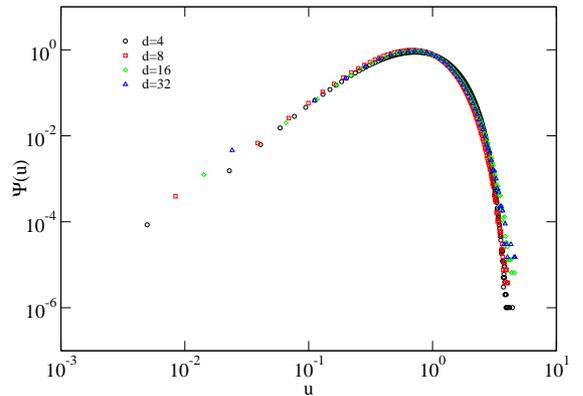


FIG. 8: After rescaling the distributions of depinning forces corresponding to distances $d = 4, 8, 16, 32$ collapse onto a unique universal master curve.

## D. Subcritical sites along the depinning front

In Fig. 9 we show the distribution of all individual depinning forces $F_i = \gamma_i - F_i^{el}$ along the front obtained from extremal dynamics. We see clearly that two different populations of sites can be distinguished. Above threshold $F^*$, $\mathcal{Q}(F > F^*)$ follows some kind of truncated Gaussian distribution. We also note that there is a small but significant number of sites which carry a force smaller than threshold, $F < F^*$. Moreover, the decay of frequency is very abrupt right below $F^*$. We will argue that this decay can be rationalized as a power-law of the difference $(F^* - F_c)$, $\mathcal{Q}(F < F^*) \propto A(L)(F^* - F)^{-\varepsilon}$. In the insert of Fig. 9 we plotted the proportion of subcritical sites $\mathcal{Q}(F < F^*)$ against the system size. This evolution appears to follow a power law $\mathcal{Q}(F < F^*) \propto L^{D-1}$ with $D \approx 0.35$. We show below that $D$ can be regarded as a fractal dimension of the set of subcritical sites along the front.

In the Appendix, we will introduce a mean-field version of the model where such a distribution can be computed analytically. In this simple variant of the depinning model, the elastic force is not transfered from the active site to its nearest neighbors but to two sites chosen randomly along the front. Although a quantitative comparison can not be established because of the mean-field nature of the solvable model, on a qualitative ground, the main features of the force distribution are recovered. On Fig 10, one can distinguish again between a Gaussian-like distribution for depinning forces above the critical threshold and a singular part below the threshold. Moreover it can be shown that the amplitude of this singular part is system size dependent.

The "subcritical" sites which carry a force smaller than threshold, play a very important role, as we now try to clarify. At each time step, the extremal site corresponds to the minimum force and always remains smaller than $F^*$. Thus the active site is always part of the subcritical sites. Its depinning induces a local unloading and an
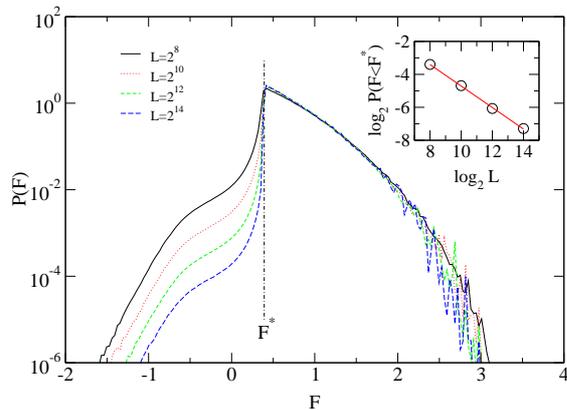
FIG. 9: Distribution of individual depinning forces $F_i = \gamma_i - F_i^{el}$ along the front. The subcritical part of the distribution $(F < F^*)$ is size dependent. In the insert we see that the relative weight of this subcritical part follow a power law of exponent 0.65 with the size $L$. This suggests that the set of subcritical site is fractal with a dimension $D = 1 - 0.65 = 0.35$

additional re-loading on its neighbors. We note that a subcritical site has a chance of being activated wherever it is located, while a site carrying a force larger than threshold can only become active if one of its neighbors become active itself. These sites can thus be regarded as a population of "precursors" of depinning.

In order to determine the distribution of the depinning forces along the front we use the same tools as above. We first show that the distribution of $F_i$ along these sites depends on their distance to the extremal one as a power law: $\mathcal{Q}(F_i < F^*) \propto |x_i - x_{i^*}|^{-a'}$. We observe then that the conditional distribution $\mathcal{Q}(F_i < F^*; |x_i - x_{i^*}| = d)$ obeys the same scaling as the one studied above for the distribution of depinning forces. This allows finally to estimate the power law behavior of the distribution of the depinning forces of this population of subcritical sites close to threshold.

On Fig. 11 we plot in logarithmic scale the mean difference to threshold $\langle F^* - F_i; |x_i - x_{i^*}| = d \rangle$ for sites at a distance $d$ from the extremal one $i^*$. We obtain the same scaling as for the distribution of the depinning force $F_c$ conditioned by the distance between successive depinning sites:

$$\langle F^* - F_i; |x_i - x_{i^*}| = d \rangle \propto d^{-\frac{1}{\nu}}, \quad \frac{1}{\nu} = 2 - \zeta \quad (16)$$

and again we see on Fig. 12 that we can rescale all conditioned distributions onto a single master curve provided the distance $d$ is large enough.

$$P\left(F^* - F_i = f > 0; |x_i - x_{i^*}| = d\right) = d^{\frac{1}{\nu}} \varphi\left(f d^{\frac{1}{\nu}}\right) \quad (17)$$

On Fig. 13 we show that the subcritical sites are not homogeneously distributed along the front. We plot in logarithmic scale the distribution of distances $d$ along the front between the extremal site and any other subcritical site. The straight line obtained in logarithmic scale

indicates that the latter obeys a power law:

$$n\left(|x_{i^*} - x_i| = d; F < F^*\right) \propto d^{-c}, \quad (18)$$

with $c \approx 0.68$, what indicates that the subcritical sites form a fractal set of dimension $D = 1 - c \approx 0.32$, which is consistent with the value $D \approx 0.35$ obtained above for the evolution of the population of subcritical sites against the system size.

The above scaling relationships can now be used to estimate the distribution of depinning forces along the front close to threshold:

$$\begin{aligned}
Q(F^* - F_i = f > 0) & \qquad (19) \\
= A(L) \int Q(F^* - F_i; \ell) n(\ell) \mathrm{d}\ell \\
= A(L) \int \ell^{\frac{1}{\nu}} \phi\left[(F^* - F_i)\ell^{\frac{1}{\nu}}\right] \ell^{-c} \mathrm{d}\ell \\
= A(L) (F^* - F_i)^{-1 + c\nu - \nu} \int u^{1 - c\nu + \nu - 1} \psi(u) \mathrm{d}u \\
\propto A(L) (F^* - F_i)^{-\varepsilon}
\end{aligned}$$

with $\varepsilon = 1 + \nu D \approx 1.45$. The size dependent prefactor can be estimated using the fact that for a front of size $L$ the typical cut-off of the elastic force is $L^{-1/\nu}$. Rewriting the total number of sub-critical sites along the front then gives:

$$\begin{aligned}
\mathcal{N}(L) & = LA(L) \int_{-\infty}^{L^{-\frac{1}{\nu}}} (F^* - F_i)^{-\varepsilon} & (20) \\
& = LA(L) L^{-\frac{1}{\nu}(1-\varepsilon)} & (21) \\
& = A(L) L^{1+D} & (22)
\end{aligned}$$

The fractal dimension of this population of subcritical sites being $D$, we have in addition $\mathcal{N}(L) \propto L^D$ which imposes $A(L) \propto L^{-1}$ and we have finally (see Fig. 14):
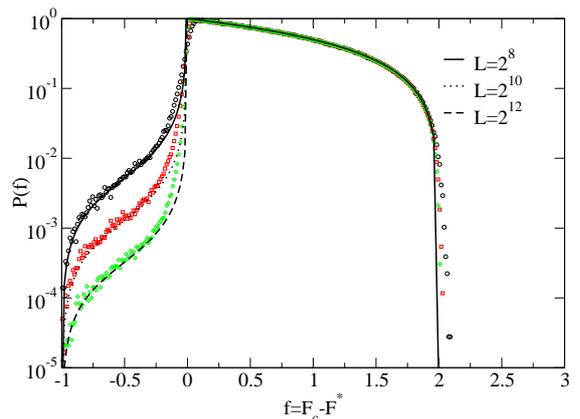


FIG. 10: Comparison between the result of a direct numerical simulation (symbols) and the previous analytic expressions (continuous curves). The system size was set to $L = 2^8, 2^{10}$ and $2^{12}$. As above we see that only the subcritical part is size dependent
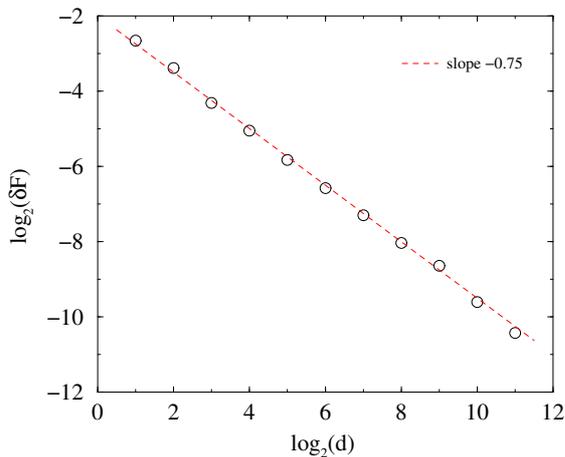
FIG. 11: The difference $\delta F$ (current force to threshold) of precursory sites located at a distance $d$ from the extremal site scales as a power law of $d$. The straight line corresponds to a power law of exponent $0.75 \approx 2 - \zeta$.
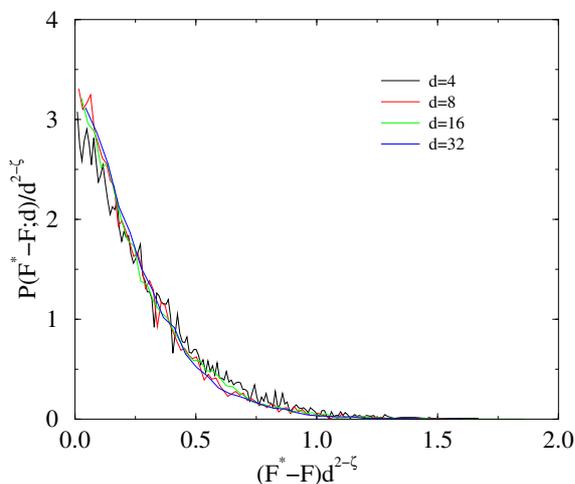


FIG. 12: After rescaling the distributions of subcritical depinning forces $F_i$ conditioned by the distance $d$ to the extremal site $i^*$, collapse onto a single master curve.

$$Q(F^* - F_i = f > 0) \propto \frac{1}{L} \left(F^* - F_i\right)^{-\varepsilon} , \quad \varepsilon = 1 + \frac{D}{2 - \zeta} \tag{23}$$

We see thus that the depinning is controlled by the evolution of a very tiny fraction of subcritical sites. These sites are distributed fractally along the front and can be regarded as precursors of the avalanches to come. Close to threshold the depinning force associated to these sites is power law distributed with an exponent depending both on the roughness exponent of the front $\zeta$ and the fractal dimension $D$ characterizing the population of subcritical sites.

## III. FINITE TEMPERATURE DYNAMICS

We now consider the case of depinning at finite temperature. The transition loses its critical character. As a matter of fact, even at arbitrary low external driving, the front keeps moving. The velocity is however extremely low, most of the time being spent to thermally depin from blocked conformations. This creep motion has been intensively studied in recent years from the experimental [3] and theoretical points of view [13, 14, 15, 16]. It has been argued that at very low forcing, the velocity follows a stretched exponential behavior against the driving force:

$$v(F, T) \propto \exp\left[-\left(\frac{F^*}{F}\right)^m \frac{T}{T_0}\right] \tag{24}$$

where $m = (2\zeta - 1)/(2 - \zeta)$. To our knowledge, the anomalous force scaling predicted in Eq. (24) has not been reproduced so far by numerical simulations[22, 23].

Note again that such a behavior is only expected to happen at very low forcing. This means in particular that the macroscopic motion of the front results from a balance between microscopic backward and forward motions.

In this section we focus our study on a slightly different situation, namely, a driving force in the vicinity of the critical threshold. This allows to neglect the probability of a backward motion. At finite temperature the motion consists of a series of rapid finite moves interrupted by long pinned stages from which the front can only escape by thermal activation. Two limit cases can actually be distinguished regarding the thermal depinning of a blocked conformation of the front. At very low temperature, the front most likely depins at the extremal site. Thus the sequence of depinning events is not affected by the introduction of a temperature. The computation of the time spent by the front to escape any blocked conformation allows however to reintroduce a physical time
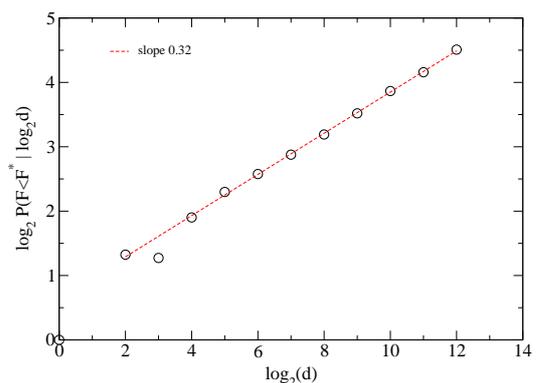


FIG. 13: Distribution $n(d)$ of distances $d$ of subcritical sites to the extremal site. The straight line indicates a power law of exponent 0.32. The data being obtained with a logarithmic sampling of $d$, this corresponds to a power law $n(d) \propto d^{-c}$, $c \approx 1 - 0.32 \approx 0.68$
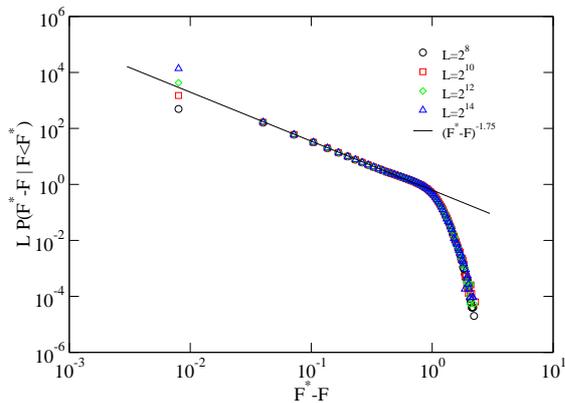
FIG. 14: Distribution of subcritical depinning forces $F < F^*$ along the front. Close to threshold the distribution of subcritical sites follow a power law of exponent $-1.75$.
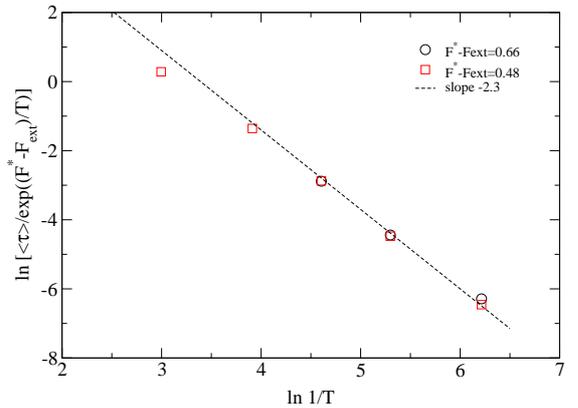


FIG. 15: Dependence of the mean waiting time on the temperature after rescaling by the dominant Arrhenius factor. The straight line indicates a power law behavior of exponent 2.3 to compare with the value $(a-1)\nu \approx 2.6$ obtained in Eq. 32 for the low temperature dynamics.

in this quasi extremal dynamics. The knowledge of the depinning force distributions $P(F_c)$ thus serves to quantify the velocity of the front. The second limit case corresponds to high temperatures. During a transient, all sites are free to advance; then the curvature of the front becomes comparable to the temperature and the dynamic of the front is rather well described by an annealed dynamics. This induces a scaling of the front roughness different from the one obtained at zero temperature: we observe a roughness exponent $\zeta_T \approx 0.5$ instead of the zero temperature value $\zeta \approx 1.25$.

In the following we first present the simple Monte Carlo algorithm used to run the dynamics of the front at finite temperature. The latter is obtained by allowing activated depinning along the front. We then give results obtained in the low and high temperature limits. We finally present a criterion allowing to discriminate between these two regimes. It appears actually that beside the "static" correlation length $\xi$ of the critical transition another characteristic length of thermal origin $\xi_T$ plays a key role in the problem: below $\xi_T$ the front follows a $T = 0$ dynamics but above $\xi_T$ the activated depinning become dominant and the front follows an annealed Edwards-Wilkinson like dynamics[24].

## A. A simple Monte-Carlo algorithm for depinning at finite T

Let us come back to the definition of the dynamics. Consider a point $i$ along the front. At zero temperature the criterion for depinning at this particular site is:

$$D_i = F^{ext} + F_i^{el} - \gamma_i > 0 \qquad (25)$$

Note here that for the sake of simplicity we only consider the fluctuating part of the random traps, the constant part, call it $\Gamma$ being implicitly absorbed in the external driving force: $F^{ext} = F^{ext}_{(0)} - \Gamma$. The values of this effective driving force may thus be arbitrarily low

and even negative without violation of the hypothesis of microscopic forward motion mentioned above.

At finite temperature we can estimate the local depinning time $t_i$ via an Arrhenius term:

$$p(t_i) = \frac{1}{\tau_i} \exp\left(-\frac{t_i}{\tau_i}\right) , \quad \tau_i = \frac{1}{\nu_0} \max\left[1; \exp\left(\frac{-D_i}{T}\right)\right] \qquad (26)$$

where $\nu_0$ corresponds to a natural frequency of vibration at the microscopic scale.

From the numerical point of view we can use the following algorithm. At time $t$, all points satisfying the criterion of propagation (25) are advanced simultaneously up to the next traps. The waiting times $\tau_j$ corresponding to the points $j$ that do not satisfy the criterion are computed from their respective distributions. Points such that the waiting time is below the time unit are also advanced. The elastic forces are then updated and time is incremented. If no point along the front has been advanced, the location of the first site to thermally depin and the associated waiting time are drawn from the Arrhenius distributions. Again the selected point moves forward, the elastic forces are updated along the front but the time is incremented by the waiting time spent in this blocked conformation. Let us now be more explicit about the determination of the waiting time and the location of the depinning site in the case of a blocked conformation.

The probability $P_i(t)dt$ that the site $i$ is the first to thermally depin in the time interval $[t, t + dt]$ can be written:

$$P_i(t) = \frac{1}{\tau_i} \exp\left(-\frac{t}{\tau_i}\right) \prod_{j\neq i} \int_t^\infty \frac{1}{\tau_j} \exp\left(-\frac{u}{\tau_j}\right) du \qquad (27)$$

$$= \frac{1}{\tau_i} \exp\left(-\frac{t}{\tau^*}\right) , \quad \frac{1}{\tau^*} = \sum_j \frac{1}{\tau_j} \qquad (28)$$

The probability $r_i$ that the activated depinning event

takes place at this particular site $i$ is thus independent of time

$$r_i = \int_0^\infty P_i(t)\mathrm{d}t = \frac{\tau^*}{\tau_i} \qquad (29)$$

In a similar manner, the probability $P_{act}(t)$ that the first activated depinning event takes place at time $t$ is

$$P_{act}(t) = \frac{1}{\tau^*} \exp\left(-\frac{t}{\tau^*}\right) \qquad (30)$$

Note that the time $t$ and location $i$ appear as independent variables. When the front is pinned, the algorithm thus consists of drawing a waiting time from the distribution $P_{act}(t)$ and to choose the site of depinning according to the weights $r_i$. The characteristic times involved in $r_i$ depend on the distribution $P(F_i)$ of individual depinning forces along the front. In the following we focus on the two limiting cases of low and high temperature.

At low temperature, when the front is pinned the waiting time is dominated by the characteristic time of the extremal site. The sequence of depinning events is identical to the one of the extremal dynamics. The time evolution directly results from the knowledge of the distribution of depinning forces $P(F_c)$ of the extremal. At high temperature, the probability of depinning becomes comparable for all sites along the front.

## B. Low Temperature behavior: activated extremal dynamics

We consider here the case of very low temperature. The loading external force $F_{ext}$ is constant below the threshold $F^*$. At a given conformation of the front, all sites satisfying the criterion of propagation are advanced, the elastic forces are then updated. If the front is blocked the only site to depin is the extremal one. The time $\tau$ associated to an iteration is drawn from an Arrhenius distribution

$$p(\tau) = \frac{1}{\tau} \exp\left(-\frac{\tau}{\tau_c}\right), \quad \tau_c = \frac{1}{\nu_0} \max\left[1; \exp\left(\frac{F_{ext} - F_c}{T}\right)\right] \qquad (31)$$

The knowledge of the distribution of depinning forces $P(F^* - F_c)$ gives us directly the distribution of waiting times in blocked configurations[25]. The mean waiting time $\langle\tau\rangle$ to depin from a blocked conformation for an external constant loading $F_{ext}$ is

$$\langle\tau\rangle = \int_{Fext}^{F^*} \mathrm{d}F_c \exp\left(\frac{F_c - F_{ext}}{T}\right) A(F^* - F_c)^\mu \qquad (32)$$

$$= T^{\nu(a-1)} \exp\left(\frac{F^* - F_{ext}}{T}\right) \qquad (33)$$

where we used the condition $T \ll F^* - F_{ext}$ to truncate the integral in the numerator. In this regime we
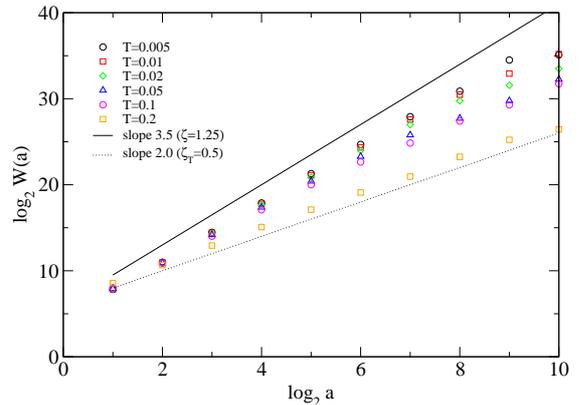


FIG. 16: Mean wavelet coefficients obtained for the depinning front driven at $F_{ext} = 0$, ($F^* - F_{ext} = 0.569$) for various temperature. The straight lines indicate the two limit behaviors of roughness exponents $\zeta = 1.25$ and $\zeta_T = 0.5$ corresponding to the critical state for temperatures close to zero a "SOS-like" behavior for higher forces. System size $N = 4096$, $32\ 10^6$ iterations.

observe a simple Arrhenius behavior for the mean depinning time with a power law correction in the ratio temperature/distance to threshold. On Figure 15 we show the scaling of this waiting time. After rescaling by the Arrhenius factor we observe indeed a power law dependence on the temperature. Numerically we find for the exponent $\nu(a - 1) = 2.3$ to compare with the expected value $\nu(a - 1) = 2.6$ with $\zeta = 1.25$ and $a = 2.95$.

## C. High Temperature behavior: Edwards-Wilkinson like dynamics

At high temperature, all growth probabilities tend to be equal, which generates an independent evolution at each site. The result is simply a white noise morphology, with ever increasing slopes and curvatures. This regime can only be a transient one. At long times (and at lower temperatures), a bias between the growth probability and the curvature will be felt and hence, this limit will correspond to an annealed model known as the Edwards-Wilkinson (EW) model[24], which indeed give rise to self-affine fronts with a roughness exponent $\zeta = 0.5$. We thus expect to see a cross-over from $\zeta = 1.25$ at small temperature, to $\zeta = 0.5$ at larger temperature. This is precisely what is observed in the numerical simulations as shown in Figure 16 which represent the scaling behavior of the front roughness for a same driving force but different temperatures. Here we measured along the front the averaged wavelet coefficients $\omega(a)$. For a self-affine front of roughness exponent $\zeta$, these coefficients are expected to scale as $\omega(a) \propto a^{1+2\zeta}$ with the length scale $a$[18]. In $\log - \log$ scale we observe a scaling behavior with an apparent exponent decreasing from $\zeta \approx 1.25$ toward $\zeta \approx 0.5$ for growing temperatures.
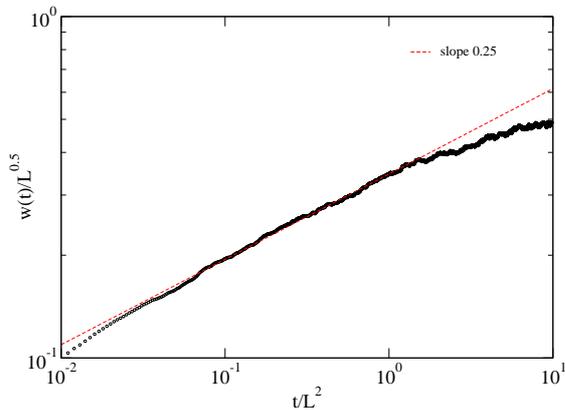
FIG. 17: Time evolution of the interface width at high temperature ($T = 0.1$) with a low forcing $F^* - F_{ext} = 0.39$. The time and height coordinates are rescaled by $L_{EW}^z$ and $L^{\zeta_{EW}}$ respectively. The value $z_{EW} = 2$ and $\zeta_{EW} = 0.5$. The evolution of the width is well described by the power law $w(t) \propto t^{\beta_{EW}}$ with $\beta_{EW} = 0.5$ (dashed lines). These critical exponents are consistent with a growth of the Edwards-Wilkinson type.

To check that this high-temperature behavior indeed belongs to the EW universality class, we show on Fig. 17 the time evolution of the interface width after rescaling of the time by $L^z$ and $L^\zeta$ with $z = 2$ and $\zeta = 0.5$. As expected in a EW growth model we observe a power law behavior with an exponent $\beta = 0.25$.

### D. Transition from low to high temperature: thermal characteristic length

Let us now consider intermediate temperatures. We can actually establish a quantitative criterion to discriminate between low and high temperature behavior.

As stated above the probability of depinning of a pinned configuration derives from the distribution of depinning forces along the front. These depinning forces can be ranked from the smallest (the extremal site) to the largest one. The extremal site is denoted $i^*$ and the associated depinning force is $F_c$. The second smallest is $i_2$ and the corresponding force is $F_{i_2}$. The typical depinning time $\tau^*$ is:

$$\frac{1}{\tau^*} = \sum_i \frac{1}{\tau_i} = \frac{1}{\tau_{i^*}} \left( 1 + \sum_{j=2}^N \frac{\tau_{i^*}}{\tau_{i_j}} \right) \quad (34)$$

where

$$\frac{\tau_{i^*}}{\tau_{i_j}} = \exp\left( \frac{F_{ext} - F_c}{T} - \frac{F_{ext} - F_{i_j}}{T} \right) = \exp\left( \frac{F_{i_j} - F_c}{T} \right) \quad (35)$$

We see here that the relative weights corresponding to the different sites do not depend on the level of external driving but only on the difference of force to the extremal

one. It is thus clear that as soon as $F_c - F_{i_j} \gg T$ the waiting time $\tau^*$ is dominated by the extremal time $\tau_{i^*}$. The ranking allows to restrict to the criterion:

$$F_c - F_{i_2} \gg T \quad (36)$$

The previous section gave us the knowledge on the distribution of depinning forces along the front, namely:

$$Q(F^* - F_i) \propto \frac{1}{L}(F^* - F_i)^{-\varepsilon} \quad (37)$$

We may thus estimate the typical difference between the two smallest depinning forces along the front:

$$\int_{F_c}^{F_{i_2}} \frac{1}{L^D}(F^* - F)^{-\varepsilon}\mathrm{d}F = \int_{F^* - F_{i_2}}^{F^* - F_c} \frac{1}{L^D}x^{-\varepsilon}\mathrm{d}x \approx \frac{1}{L^D} \quad (38)$$

where $1/L^D$ in the integral is a normalizing factor of the subcritical force distribution and $L^D$ at the right hand sides is the number of subcritical site. A Taylor expansion around $F_c$ leads to

$$(F_c - F_{i_2}) \approx (F^* - F_c)^\varepsilon \quad (39)$$

We see in Fig. 18 that this scaling is nicely observed with the value $\varepsilon = 1.7$ consistent with the estimation obtained above for the distribution of subcritical depinning forces. The extremal value of the depinning force $F_c$ is a fluctuating quantity during the course of the propagation. In the first part of this paper we saw that the difference $F^* - F_c$ can be associated to a typical distance $d$ between consecutive depinning sites by the scaling $d \propto (F^* - F_c)^{-\nu}$. The criterion for extremal depinning during the propagation can thus be characterized by a distance $\xi_T$ below which the activated site is the extremal one and above which the activated site is randomly chosen along the front:

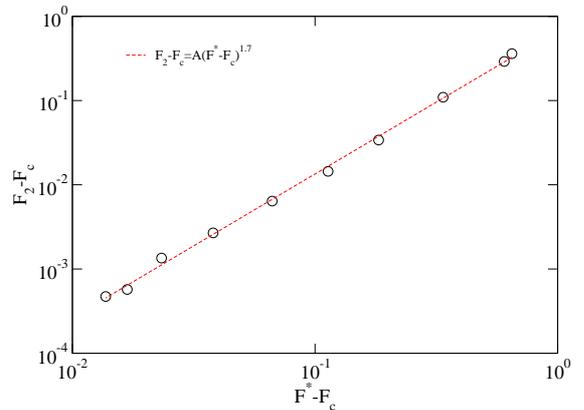$$\xi_T \propto T^{-\frac{\nu}{\varepsilon}} \quad (40)$$



FIG. 18: Difference between the two smallest depinning forces $F_2 - F_c$ along the front against the difference $F^* - F_c$. The data are well described by power law of exponent $\varepsilon = 0.7$.
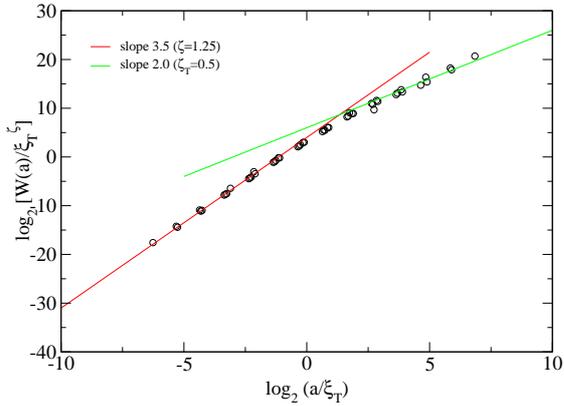
FIG. 19: After rescaling the abscissa by the characteristic length $\xi_T \propto T^{-\nu/\epsilon}$ with $\nu = 1.33$ and $\epsilon = 1.4$, and the ordinate by $\xi_T^\zeta$ with $\zeta = 1.25$, the mean wavelet coefficients obtained for the depinning front driven at the constant driving force $F_{ext} = 0$, $(F^* - F_{ext} = 0.569)$ for different temperatures collapse onto a single master curve.

In Fig. 16, we presented the scaling of the front roughness obtained for a constant forcing at various temperatures. As expected, the scaling evolves from the zero temperature behavior $\zeta = 1.25$ to an annealed behavior $\zeta = 0.5$: the various curves are distributed between these two limit cases. However, rescaling the lateral length by the temperature dependent characteristic length $\xi_T$, we can collapse all results onto a single master curve (see Fig. 19) where the small arguments correspond to the critical behavior and the large arguments to the annealed behavior.

## IV. CONCLUSION

We studied the depinning of an elastic line in strong pinning conditions.

In a first part we focused on the critical behavior at zero temperature, based on an extremal dynamics to perform numerical simulations. Beyond the scaling properties of the front roughness and the avalanche dynamics observed at the depinning transition our main results concern the statistics of the depinning forces. At each conformation of the front we can associate the minimum force $F_c(t)$ needed to depin the front. The distribution of these depinning forces present a singular behavior in the vicinity of its maximum value, the critical threshold $F^*$ is $P(F_c) \propto (F^* - F_c)^\mu$ where the critical exponent $\mu$ directly depends on the roughness exponent $\zeta$ of the depinning front. Moreover this distribution relative to large jumps $d$ in the activity adopts a universal form for all values of $F$.

Moreover it appeared that the critical dynamics concentrates on a very tenuous set of sites (termed subcritical) along the front, in fact a fractal structure. Beyond neighboring effects, the critical site is always chosen

among this set. The latter can thus be regarded as precursors of the future avalanches. All of these sites are characterized by a sub-critical depinning force, namely the force $F$ needed to make them move is below the critical threshold $F^*$. Again the distribution of the depinning forces associated to these precursory sites presents a universal character: $P(F) \propto L^{-1}(F^* - F)^{-\epsilon}$, again composed of a universal form when conditioned by the distance to the active site.

In a second part we extended the study of the depinning transition at finite temperature. The front was driven at a constant below threshold driving force. A simple Monte-Carlo algorithm was developed to simulate the activated dynamics.

Two limit cases were considered. At very low temperature or at small scale, the extremal site is by far the most probable site to depin and all critical properties are preserved. In this limit, the finite temperature then mimics the extremal dynamics. Assuming an Arrhenius behavior for the depinning from any individual trap we are able to associate a physical time to this quasi extremal dynamics. The knowledge of the depinning force distribution $P(F_c) \propto (F^* - F_c)^\mu$ then allows a quantitative estimate of the front velocity. We recover a simple Arrhenius dependence with a temperature power law dependence. At high temperature or at large scales, all sites can equally be activated. This annealed dynamics has been shown to be well described by an Edwards-Wilkinson growth model. The transition between these two regimes can be estimated using the ratio of the temperature to the gap between the two smaller depinning forces. We showed that this gap can be naturally associated to a temperature dependent characteristic length along the front $\xi_T \propto T^{-1/\epsilon\nu}$. Below the characteristic length $\xi$ the front adopts naturally a critical dynamics, at larger scales the annealed dynamics dominates.

## APPENDIX A: A SOLVABLE MEAN FIELD DEPINNING MODEL

We present in this appendix a mean field variant of the extremal depinning model studied in section II. We first note that we can set all thresholds to 0, and provided that the moves are still random, the behavior remains similar. In this context the extremal site $i^*$ simply minimizes the local elastic force:

$$F_c = F_{i^*}^{el} = \min_i F_i^{el} . \qquad (A1)$$

Once the extremal site has been determined the front advances up to the next trap. However we introduce here a change in the definition of the elastic forces. In the original Laplacian version $F_i^{el} = -h_{i-1} + h_i - h_{i+1}$, the extremal site is unloaded proportionally to the local displacement just covered and conversely its two nearest neighbors are equally loaded. In the mean field version

we present here, the two sites loaded to keep the elastic force balance are chosen randomly along the front, hence the term mean field.

Let us call $x$ the gap between the local elastic force and the critical threshold, $x = F^{el} - f^*$, $p(x)$ its distribution density, and $P(x)$ the cumulative probability $P(x) = \int_x^\infty p(y)dy$ (from which $p(x) = -P'(x)$ results).

For a system of size $L$, the smallest $x$ has a density $p_s(x)$ and cumulative $P_s(x)$. We have $P_s(x) = P(x)^L$, and thus $p_s(x) = LP(x)^{L-1}p(x)$.

Ignoring spatial correlations, we can write a mean-field master equation for $p(x)$.

$$
\begin{aligned}
\frac{dp(x)}{dt} &= -p_s(x) - 2p(x) \\
&\quad +(1/2)\int_0^2 p_s(x-y)dy \\
&\quad +2\int_0^1 p(x+y)dy \\
&= -p_s(x) - 2p(x) \\
&\quad +(1/2)(P_s(x-2) - P_s(x)) \\
&\quad +2(P(x) - P(x+1))
\end{aligned} \tag{A2}
$$

The terms of the right hand side correspond to the probability of occurrence of the following events $i)$ $x$ is the extremal value of the elastic force along the site; $ii)$ Before the update, one of the two random sites to be loaded carried a force $x$; $iii)$ After update the advancing site carries a force $x$; $iv)$ After update one of the two random sites carries a force $x$.

In the steady state, we have

$$
-2P'(x)-P_s'(x) = (1/2)(P_s(x-2)-P_s(x))+2(P(x)-P(x+1)) \tag{A3}
$$

In order to integrate this equation, we distinguish in the following between three different intervals. The region 1 $(x < 0)$ corresponds to the subcritical sites. The region 3 $(x > 1)$ corresponds to deeply pinned sites which have no chance to become neither subcritical nor critical at the next depinning event. The intermediate region 2 $(x > 1)$ exchanges with the two other ones. For $x < 0$,

we expect $P(x)$ to be equal to 1 but a small correction vanishing as $L$ diverges. $P(x) = 1 - \Psi_L(x)$. We look for $\Psi_L(x) = (1/L)\Phi(x)$. Thus $P_s(x) = (1 - (1/L)\Phi(x))^L \rightarrow \exp(-\Phi(x))$. The equations corresponding to the three regions write:

- Part 1:

$$
-P_s'(x) = (1/2)(1 - P_s(x)) + 2(1 - P(x+1)), \quad (x < 0) \tag{A4}
$$

- Part 2:

$$
-P'(x) = P(x) - P(x+1) + (1/4), \quad (0 < x < 1) \tag{A5}
$$

- Part 3:

$$
-2P'(x) = (1/2)P_s(x-2) + 2P(x), \quad (x > 1) \tag{A6}
$$

and the solutions are respectively

- Part 1: $(x < 0)$

$$
P_s(x) = -x^2 - 2x, \tag{A7}
$$
$$
P(x) = 1 - \frac{1}{L}\frac{2(x+1)}{x(x+2)}, \tag{A8}
$$

- Part 2 and 3: $(x > 0)$

$$
P(x) = (1/4)(x-2)^2. \tag{A9}
$$

These analytical expressions are compared with numerical results on Fig. 10. Beyond the excellent agreement between analytics and numerics, the similarity between Fig. 9 and 10 shows that this simple mean field model allow to recover the main feature of the original model. The distribution of local depinning forces is composed of a size independent supercritical part and of a size dependent subcritical part which presents in addition a singular behavior close to the forces approach the critical threshold.

[1] S. Moulinet, C. Guthmann, and E. Rolley, Eur. Phys. J. E **8**, 437 (2002).
[2] K. Måløy and J. Schmittbuhl, Phys. Rev. Lett. **78**, 3888 (1997).
[3] S. Lemerle, J. Ferré, C. Chappert, V. Mathet, T. Giamarchi, and P. L. Doussal, Phys. Rev. Lett. **80**, 849 (1998).
[4] H. Leschhorn, T. Nattermann, S. Stepanow, and L.-H. Tang, Ann. Phys. (Leipzig) **6**, 1 (1997).
[5] M. Kardar, Phys. Rep. **301**, 85 (1998).
[6] D.-S. Fisher, Phys. Rep. **301**, 113 (1998).
[7] K. Sneppen, Phys. Rev. Lett. **69**, 3359 (1992).
[8] H. Leschhorn and L.-H. Tang, Phys. Rev. E **49**, 1238 (1994).
[9] J. Schmittbuhl, S. Roux, J. Vilotte, and K. Måløy, Phys. Rev. Lett. **74**, 1787 (1995).
[10] A. Tanguy, M. Gounelle, and S. Roux, Phys. Rev. E **58**, 1577 (1998).
[11] R. Dickman, M. A. Muñoz, A. Vespignani, and S. Zapperi, Braz. J. Phys. **30**, 27 (2000).
[12] O. Narayan, Phys. Rev. E **62**, R7563 (2000).
[13] M. Feigel'man, V. Geshkenbein, A. Larkin, and V. Vinokur, Phys. Rev. Lett. **63**, 2303 (1989).
[14] M. M. V. M. Vinokur and L.-W. Chen, Phys. Rev. Lett. **77**, 1845 (1996).
[15] P. Chauve, T. Giamarchi, and P. L. Doussal, Phys. Rev. B **62**, 6241 (2000).
[16] T. Nattermann and S. Scheidl, Adv. Phys. **49**, 607

(2000).

[17] D. Vandembroucq and S. Roux, preprint (2003).

[18] I. Simonsen, A. Hansen, and O. Nes, Phys. Rev. E **58**, 2779 (1998).

[19] J. Lopez, M. Rodriguez, and R. Cuerno, Phys. Rev. E **56**, 3993 (1997).

[20] S. Krishnamurthy, A. Tanguy, and S. Roux, Eur. Phys. J. B **15**, 149 (2000).

[21] S. Krishnamurthy, A. Tanguy, P. Abry, and S. Roux, Europhys. Lett. **51**, 1 (2000).

[22] L.-W. Chen and M. Marchetti, Phys. Rev. B **51**, 6296 (1995).

[23] L. Roters, S. Lübeck, and K. Usadel, Phys. Rev. E **63**, 026113 (2001).

[24] A. Barabasi and H. Stanley, *Fractal Concepts in Surface Growth* (Cambridge Univ. Press, 1995).

[25] R. Skoe, D. Vandembroucq, and S. Roux, Int. J. Mod. Phys. C **13**, 751 (2002).